



HAL
open science

Steep Bedload-laden Flows: Near-Critical?

Guillaume Piton, Alain Recking

► **To cite this version:**

Guillaume Piton, Alain Recking. Steep Bedload-laden Flows: Near-Critical?. Journal of Geophysical Research: Earth Surface, 2019, 124 (8), pp.2160-2175. 10.1029/2019jf005021 . hal-02266073

HAL Id: hal-02266073

<https://hal.science/hal-02266073>

Submitted on 13 Aug 2019

HAL is a multi-disciplinary open access archive for the deposit and dissemination of scientific research documents, whether they are published or not. The documents may come from teaching and research institutions in France or abroad, or from public or private research centers.

L'archive ouverte pluridisciplinaire **HAL**, est destinée au dépôt et à la diffusion de documents scientifiques de niveau recherche, publiés ou non, émanant des établissements d'enseignement et de recherche français ou étrangers, des laboratoires publics ou privés.

Steep Bedload-laden Flows: Near-Critical?

Guillaume PITON ^{*1} and Alain RECKING¹

¹Univ. Grenoble Alpes, Irstea, Grenoble center, UR ETNA, Grenoble, France.

August 13, 2019

This is the personal first author's version of a paper published in *Journal of Geophysical Research: Earth Surface*. To cite the paper:

Piton, G. & Recking, A. (2019). Steep Bedload-laden Flows: Near-Critical? *Journal of Geophysical Research: Earth Surface*, DOI:10.1029/2019JF005021

- Bedload-laden flume flows show autogenic cycles of braided depositional patterns alternating with erosive single-channel morphologies
- Froude numbers were mostly subcritical despite steep slope
- Near-critical or slightly supercritical flows can occur in steep, unconfined reaches with intense bedload transport

Abstract

Steep gravel-bed rivers sometimes experience floods that dramatically rework river bed structure and topography. Hazard assessments and paleo-event reconstructions require better knowledge of such phenomena. This paper explores morphodynamic evolution of steep channels carrying bedload-laden flows, using a generic Froude-scaled model. Bedload-laden floods were introduced in a narrow flume and spread into a five-times wider unconfined area with a 0.1-step slope (m/m). Image analysis enabled measurements taken at an unprecedented level of accuracy on unconfined flows laden with bedload. A flow reconstruction procedure was used to compute depth, Froude (Fr) and Shields (τ^*) numbers on millions of pixels based on a friction law and measurements of surface velocity, slope, and roughness. Despite the steep slope, Froude numbers proved to be mostly subcritical in all but the regions experiencing the most active sediment transport. Competent flows, identified by the transport stage higher than unity ($\tau^*/\tau_{cr}^* > 1$), were near-critical and seldom had $Fr > 1.3 - 1.5$. This demonstrates that, providing that bed width and structure can adjust, hydraulic features such as standing waves, hydraulic jumps and lateral shock waves dissipate energy very efficiently in addition to adjusting channel features. These competent flows also tend to rework channels to approach the energy minimum of near-critical flows. This hypothesis was postulated by Gordon Grant (1997, *Wat. Resour. Res.* 33(2):349-358), but demonstrated here for the first time at this scale. Considering near-critical flows during discharges high enough to be clearly competent in laterally unconfined reaches seems reasonable as a first approximation in steep channels.

*Guillaume PITON guillaume.piton@irstea.fr

1 Introduction

Gravel-bed rivers in piedmont and mountain regions sometimes experience high-magnitude flood events dramatically reworking river bed topography and valley-bottom geometry (Arnaud-Fassetta et al. 2005; Hauer and Habersack 2009; Rickenmann and Koschni 2010; Rickenmann et al. 2015; Comiti et al. 2016; Righini et al. 2017; Ruiz-Villanueva et al. 2018; Scorpio et al. 2018). Determining flow features such as discharges, velocities, water depths, total and unit stream powers, Shields stresses and Froude numbers during such events are cornerstones of a number of studies (Lumbroso and Gaume 2012). This is indeed necessary when assessing debris flood hazards and designing protection works. It is also part of paleo-event reconstructions for flood magnitude estimations. Finally, it helps improve predictive models as well as hydraulics by providing a better understanding of process-based linkages among flow features, sediment transport and channel morphology.

Grant 1997 introduced the so-called critical flow hypothesis, speculating that highly supercritical flows should be rarely or very transiently observed in the field in mobile-bed river channels. Indeed, autogenic energy dissipation processes, e.g., undular hydraulic jumps and standing waves, emerge rapidly where supercritical flows occur and dissipate kinetic energy very efficiently. A corollary of this observation is that geomorphology interacts with the flow field and forms arise, i.e., step-pools form, grains cluster and sort, bedforms adjust and the river bed may widen or narrow. As a consequence, any transient energy excess eventually dissipates by increases in bed roughness or width and thus total friction dissipation. Since critical flow is the optimum energetically speaking, the Froude-number-close-to-unity criterion should act as an attractor for flows competent enough to rework the morphology, providing that the bed geometry and structure can adjust. Typical features of near-critical flows such as standing waves, undular hydraulic jumps, and step-pools are consequently very common in the field.

Several direct field measurement campaigns implemented in mountain rivers during mean flows seldom reported highly supercritical Froude numbers (e.g. Tinkler 1997; Lenzi 2001; Zimmermann and Church 2001; Comiti et al. 2007; Comiti et al. 2009; Magirl et al. 2009; Nitsche et al. 2012; Recking et al. 2012; Schneider et al. 2015). Interestingly, most peak-flow reconstructions after moderate- to extreme-magnitude flood events were also sub- or near-critical (Rickenmann and Koschni 2010; Hauer and Habersack 2009; Lumbroso and Gaume 2012; Ruiz-Villanueva et al. 2018). Such reconstruction are usually less accurate than direct measurements because they are indirectly computed from flow modeling or post-event measurements and interpretations. Peak-flow estimations remain however key input data to many of the applications mentioned above (Lumbroso and Gaume 2012). Obviously, higher uncertainties arise if dramatic geomorphic adjustments occurred in addition to extraordinarily high flow levels.

Bedload-laden flows over very steep slopes, i.e., close to or greater than 0.1 m/m, are very complex phenomena. Several stations have monitored such creeks for decades (e.g., Rickenmann et al. 2013; Rainato et al. 2016) and recorded a few high-magnitude events on the confined reaches where the stations are located. Less data and knowledge are available for flows occurring when bedload-laden floods reach alluvial fans and lose confinement or when debris floods spread in sediment detention basins (but see Piton et al. 2018a; Theule et al. 2018). Such events have seldom been directly monitored because they are flashy, rare, often unexpected and potentially dangerous to *in situ* measurement by their capacity to destroy and damage sensors.

Although field data remain the ultimate evidence, experiments are useful to shed light on processes difficult to measure in the fields. Small-scale models enable measurement of analog conditions for high-energy flood events under controlled conditions with direct measurement of velocities, depth, bed geometry and roughness. We conducted a set of experiments to better understand the dynamics of laterally unconstrained flows loaded with poorly sorted gravels and flowing on very steep slopes (Piton 2016). The initial idea was to qualify the flow regime occurring in sediment deposition basins when debris floods fill them. A procedure designed to measure and reconstruct 2D depth-averaged flows based on this set-up and image analysis techniques was presented in Piton et al. 2018b.

The present paper reports on flow conditions emerging when bedload-laden flows reach very steep, laterally unconstrained areas. In essence, we investigate which geomorphic patterns settle in such contexts and how varied could be the range of Froude and Shields numbers of the flows upon these patterns. The paper first briefly reports the experimental set-up and reviews the flow measurement and reconstruction method. It then analyzes flow regimes and links to bed geomorphology. Finally, we discuss the critical-flow hypothesis in light of both the existing literature and these new measurements.

2 Materials and Methods

2.1 Experimental set-up

This study utilizes a "generic Froude-scale model", i.e., a scaled version of a general geomorphic feature (Peakall et al. 1996). Only a concise description of the experimental set-up and the methods are presented here; more technical details are available in Piton 2016 and Piton et al. 2018b.

The model geometry consisted of two experimental reaches: a narrow, confined and armored 15%-steep reach that transitioned into a five-times wider reach with alluvial material and a 10%-slope. This geometry may, for instance, represent a sediment deposition basin at a scale reduction of 1:15-1:50, the most representative scale being 1:25 Piton 2016, p. 158. It could also be viewed as a very simplified transition between gorges and fan in a steeply sloping creek. The flume was 6 m long, 1.25 m wide, and 0.4 m deep. All measurements were taken within the "investigation area," i.e., in the wide, 2.5-m-long lowest part of the flume (Figure 1). The transverse profile was initially flat, i.e., without a pre-existing channel, similar to recently cleaned sediment deposition basins. The inlet pipe is assumed to be an analog small-scale model of a steep torrent where bedload transport is transferred over an armored layer with no interaction and buffering of the sediment flux; its width and slope were selected with this objective in mind. Coarse grains were glued in the pipe to limit flow acceleration at the inlet. Additionally, a few cobbles were put at the basin inlet to dissipate energy (Figure 1). These cobbles break the upstream energy and confine the hydraulic jump related to the inlet pipe in its direct vicinity (see video in supplemental material).

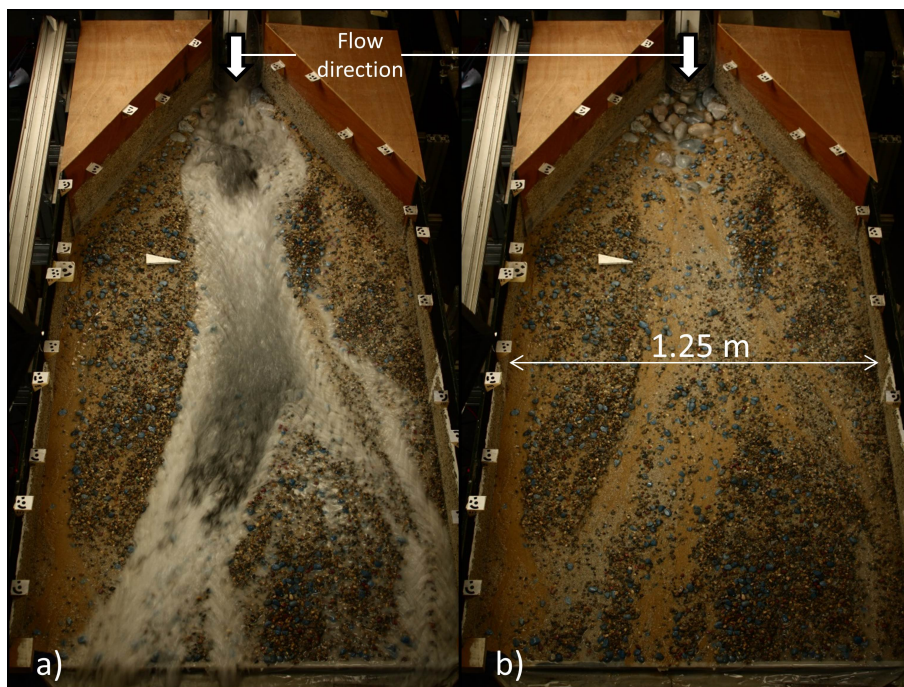


Figure 1: Images of investigation area: a) flow seeded with charcoal powder clouds during the large-scale particle image velocimetry (LSPIV) image capture, immediately followed by b) drained-bed image capture for structure-from-motion photogrammetry (SfM) acquisition. Flow reconstruction was performed at a certain distance from the inlet and outlet sections to prevent the influence of boundary conditions.

We used two sediment mixtures, with $D_{84} = 3.8$ mm and $D_{84} = 2.4$ mm, respectively, D_{84} being the 84% quantile of the grain size distribution (Table 1). We prepared them based on several sieved mixtures with diameters ranging from 0.2 mm to 20 mm. Piton 2016 compared the two mixture curve shapes with those of steep creeks, highlighting that they are consistent with natural coarse mixtures. Grains finer than 0.2 mm were not used so as to prevent colloidal effects. This means that, assuming a down-scaling of 1:25, sand smaller than 5 mm was absent, thus damping small geomorphic adjustments related to partial transport of the finest fraction (Wilcock and McArdell 1997).

Filling sediment deposition basins is partially controlled by hydrograph shape and duration (Piton and Recking 2016). We consequently used varying feeding conditions with hydrographs (Table 1). Simple triangular hydrographs

Table 1: Experimental plan

GSD code	D_{16} [mm]	D_{50} [mm]	D_{84} [mm]	Qpeak [l/s]	Qs,peak [g/s]	Tpeak [min]	C=Qs/Q [%]	N_{run}	$N_{DEM\&PIV}$	$N_{water\ depth}$
1	1.7	3.8	8.1	2.75	73-292	22.5-90	1-4	4	14	28
2	1.2	2.4	6.2	1.62-2.75	146-213	30-45	2-5	9	47	68
Total								13	61	96

Note: D_X diameter such that $X\%$ is finer, Qpeak: peak water discharge range, Qs,peak: peak sediment discharge range, Tpeak: duration before hydrograph peak, C: sediment concentration assuming a sediment density of 2.65, N_{run} : total number of hydrographs tested; $N_{DEM\&PIV}$: total number of nearly simultaneous digital elevation models (DEM) and large-scale particle image velocimetry (LSPIV) acquisition; and $N_{water\ depth}$: total number of manual point gauge water depth measurements

were used with a recession duration 1.7 times longer than the rising limb, as previously used by Armanini and Larcher 2001, for instance. Water was recirculated while sediment was fed by a hopper and a conveyor belt with controlled velocity.

For the sake of simplicity, the sediment discharge was set proportional to the water discharge using various sediment concentrations $C = Q_s/Q \in [0.01; 0.05]$, with Q and Q_s the water and sediment discharges, respectively. The minimum concentration was chosen such that deposition in the investigation area was marginal, flow merely reworking the topography. Conversely, maximum concentration triggered massive deposition, the supply maximum value being limited by the conveyor belt capacity.

The total volume of sediment injected was kept constant between runs (≈ 500 kg). Maintaining a constant total sediment supply while varying the instantaneous sediment concentration and keeping the water discharge as high as possible required changing the flood duration. As a consequence, the duration of each experiment was inversely proportional to the concentration.

2.2 Measurement set-up

Several image analysis methods were used to capture flow features: large-scale particle image velocimetry (LSPIV - Fujita et al. 1998; Muste et al. 2008) and Structure-from-Motion photogrammetry (SfM - Westoby et al. 2012) as detailed in Piton et al. 2018b. For the sake of conciseness, only a summary and complementary information are given here.

A high-speed Phototron FASTCAM camera (125 frame/s) took videos lasting a few seconds of charcoal-seeded flows (Figure 1). These pictures were used to estimate surface velocities V_{LSPIV} and subsequently depth-averaged velocities $V_{X,Y}$ using the LSPIV method and a correction factor between surface velocities and depth-averaged velocities of 0.84.

The pump was stopped while LSPIV acquisition was in progress, the flume drained in a few seconds and two CANON 100D cameras took pictures from a trolley circulating over the flume. High-quality digital elevation models (DEM) of the elevation Z for all points X, Y were reconstructed using the SfM method with the HD-pictures and photogrammetry software (Agisoft Photoscan). For every coordinate point X, Y , millimeter-accurate elevation fields $Z_{X,Y}$ (m) were built. Local slope values were computed by linear fits. Residual topography $K_{S_{X,Y}}$ was also computed by the difference between cell elevation and mean elevation on a 20-mm side square around the cell (Cavalli et al. 2008).

The elevation measurements were coupled with flow surface velocity measurements. In sum, the first step consisted of the interpolation of the flow direction at all flooded points from the LSPIV velocity measurements. We assumed that surface velocities are relevant proxies for depth-averaged flow directions and thus stream lines. The residual topography standard deviation (σ_{K_s}), called the "roughness index" by Cavalli et al. 2008, and the channel slope $S_{X,Y}$ (m/m) were extracted from the DEM specifically along the local flow direction at each point. The method provided surface velocity from which depth-averaged velocity was estimated with an assumed correction coefficient, as well as slope and bed roughness at every point of the flow, in our case on 5-mm pixels, extracted along simplified stream lines.

Before each LSPIV measurement, one or two flow depth measurements were taken with a point gauge usually near the center of one channel (Table 1). These are hereafter referred to as "reference points". Within the 13 runs performed, we undertook an accumulated number of 61 LSPIV + SfM acquisitions and an accumulated number of 96 depth measurements, i.e., 96 reference point data. Grain size distributions were also measured using Wolman 1954's counts at these locations, and D_{84} were computed. A proportionality with the roughness index was demonstrated, as in other studies (Brasington et al. 2012; Vázquez-Tarrío et al. 2017):

$$D_{84} \approx 7\sigma_{Ks} \quad (1)$$

Several friction laws relating the velocity to flow depths, slope and roughness (D_{84} or σ_{Ks}) were tested on the reference points. The Ferguson (2007) friction law proved to be the most relevant for such very shallow flows with substantial roughness, consistently with several other studies (e.g., Rickenmann and Recking 2011; Schneider et al. 2015):

$$\frac{V}{\sqrt{gdS}} = \frac{2.5(d/D_{84})}{\sqrt{1 + 0.15(d/D_{84})^{5/3}}} \quad (2)$$

with d the water depth (m) and g gravitational acceleration ($\text{m}\cdot\text{s}^{-2}$). To extend the friction law for all areas of flow, a modified Ferguson (2007) friction law was used by introducing Equation (1) into Equation (2):

$$\frac{V_{X,Y}}{\sqrt{gd_{X,Y}S_{X,Y}}} = \frac{2.5(d_{X,Y}/7\sigma_{Ks,X,Y})}{\sqrt{1 + 0.15(d_{X,Y}/7\sigma_{Ks,X,Y})^{5/3}}} \quad (3)$$

This modified Ferguson equation gave similar values to compute flow depth with the original formulation (Piton 2016; Piton et al. 2018b). Applying Equation (3) to all flowing areas makes it possible to reconstruct full depth-averaged flow features: depth d , velocity V , slope S , roughness index σ_{Ks} and equivalent grain size $D_{84} = 7\sigma_{Ks}$ (Figure 2).

In the last step, dimensionless numbers such as Froude numbers Fr and the Shields number τ^* could be computed as well, using simplified equations:

$$Fr = \frac{\alpha^{0.5} v}{\sqrt{g \cos\theta d}} \approx \frac{0.84 V_{LSPIV}}{\sqrt{g d_{X,Y}}} \quad (4a)$$

$$\tau^* = \frac{S d}{(s-1) D_{84}} \approx \frac{S_{X,Y} d_{X,Y}}{(s-1) 7 \sigma_{Ks,X,Y}} \quad (4b)$$

with α the kinetic energy correction factor approximated to 1 (-), $\theta = \text{atan}(S)$ the slope angle ($^\circ$) whose cosine ≈ 1 in river beds (3% deviation at slope 0.25) and s the sediment density taken here as 2.65 (-). See Liggett 1993 for a discussion of the Froude number estimation and averaging implied in estimations along a current line or at the cross-sectional scale. See also Magirl et al. 2009 for a practical application of Froude number computation taking into account detailed depth-wise velocity profile measurements and thus the effect of α .

This method provides a great number of reconstructed values at high resolution based on a procedure in several steps described above and summarized here (Fig. 2): (i) one or two local depth measurements (for later friction law validation); (ii) charcoal seeding and video acquisition (for later surface velocity estimation); (iii) instantaneous stopping of the pump a few seconds before the charcoal patterns reached the flume outlet; (iv) the flume was then drained in about 5 to 10 s; these four steps usually took less than 30 s (back analysis from the videos); (v) high-definition image acquisition of the dry bed (for later SfM photogrammetry reconstruction); (vi) instantaneous restarting of the pump and continuing of the experimental run. Each set of these six steps made it possible to reconstruct one map of flows on a regular grid with a 5-mm space between points in the application presented in this paper, resulting in thousands of values per DEM-LSPIV measurement. Whenever the steps took too long, the seeding was not done properly or morphological changes occurred during an abnormally long pump stoppage, the data were not used.

Uncertainties in measurements and flow depth reconstruction are discussed in depth in Piton et al. 2018b. Using a full uncertainty propagation by Monte Carlo analysis, they showed that relative uncertainty on reconstructed water depth was 15%, ignoring the friction law uncertainty. To provide here insights into uncertainties with calculations of Fr and τ^* , we performed a full error propagation procedure on the data available at reference points where uncertainties on each parameter were assessed by Piton et al. 2018b, thus providing point-specific uncertainties. We propagated the measurements' relative uncertainties using standard quadratic error propagation through Eqs. (4a) and (4b). We used (i) surface velocity uncertainties of $2\% \pm 2\%$ (mean \pm standard deviation of point-specific uncertainties), (ii) uncertainty on the surface-to-depth-averaged velocity correction factor of 4% according to data of Polatel (2006, p. 39), (iii) slope uncertainty of $19\% \pm 11\%$, (iv) roughness index uncertainties $24\% \pm 15\%$ and (v) the 15% relative uncertainty on depth. This resulted in $16\% \pm 0.4\%$ and $37\% \pm 15\%$ relative uncertainties on Fr and τ^* , respectively. It is worth stressing that the lower uncertainty associated with Fr is partially due to the nonlinearity of Eq. (4a): the square root limits the total uncertainty increase related to reconstructed depth accuracy. Conversely, τ^* is not extremely accurate, which also reinforces the need to account for sensitivity of this parameter using several filtration values (see below).

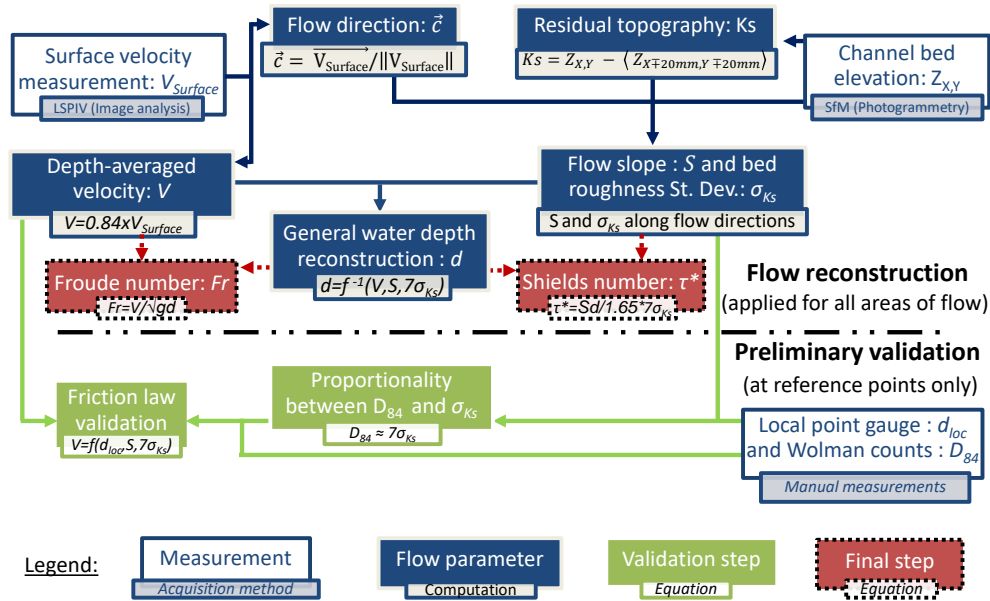


Figure 2: Flow chart summarizing the flow reconstruction procedure from LSPIV, SfM, manual measurements and friction law validation and inversion. Dark arrows map the flow parameters' intermediate computation steps, the final steps of Froude and Shields number computation are highlighted by the dotted lines, clear arrows display the validation steps of the initial procedure.

3 Results

3.1 Channel types

At the channel scale, we did not observe dune or clear antidune trains, nor step pools. Channels were mostly plane bed and cascade channels according to the terminology of Montgomery and Buffington (1997). Slopes remained steep to very steep, within a range of 0.02-0.25 (m/m). Channels varied within a wide range of widths, from a few centimeters to very transiently 0.3-0.4 m. Bedload transport intensity varied greatly in time and space. Flow velocities, depths, Froude and Shields numbers were usually higher in the central parts of channels (Fig. 3e-h). It should be emphasized that the Fr and τ^* analyses provided below are not cross-section-averaged values. Flows with high values of Fr and τ^* sometimes formed within limited sections of a channel's flow field and during short periods. Nonetheless section-averaged values of Fr and τ^* remain lower, as for 2D vs 1D depths or velocities. Identifying each channel and comparing local and cross-sectional values of Fr and τ^* is beyond the scope of this paper.

Dramatic geomorphic changes were observed during every run. Deposition and erosion formed channels, lobes, terraces and bars everywhere in the investigation area. At this scale, the deposition process was very similar to alluvial fan formation, as yet thoroughly described by Van Dijk et al. (2009) and Van Dijk et al. (2012) and Reitz and Jerolmack (2012). In essence, autogenic cycles emerged where phases of slow deposition with multi-thread channel patterns were episodically followed by fast avulsion and incision of a single-thread channel (Piton et al. 2016; Piton 2016). The cycle duration increased as the fan area grew (Reitz and Jerolmack 2012).

Braided pattern prevailed during the aggradation phases. These phases sometimes lasted dozens of minutes. Flow field and geomorphology interacted constantly to produce the hydraulics and bedforms observed. Both bed forms and bed structure regularly changed, i.e., grain packing, imbrication and clustering (Church 2006) as describing hereafter. Grain size segregation played a key role in the geomorphic changes. Aggrading and stable channels experienced intense kinetic sieving, i.e., fine grains percolating into the bed (Frey and Church 2009; Bacchi et al. 2014). Multi-thread channels were thus usually paved and steep. Their morphology was of the plane bed or cascade types according to the terminology of Montgomery and Buffington (1997). The bed was too active and mobile to develop steps and ribs. Trains of standing waves and lateral shock waves developed from both channel banks (see video in supplemental material). These braided flows were mostly subcritical despite their steepness (Fig. 3e): flows being usually shallower than in single-thread configuration and channel beds being coarser and more clustered (compare Fig. 3c & d). Energy dissipation by friction was consequently significant and prevented the flow to reach

high velocities.

Fast and transient armor-breaking events cyclically incised a single deep channel in the deposits in a few minutes. Incision occurred sometimes after an avulsion and systematically after armor breaking, thus reaching the subsurface finer material. Such armor-breaking channels were mostly covered by fine sediment and were therefore much smoother than braided channels (Fig. 1b & Fig. 3d). Bedload sheets, i.e., transient bursts of more intense sediment transport over smooth bed, were systematically observed as in Kuhnle and Southard (1988), Recking et al. (2009), and Venditti et al. (2010). A self-reinforcing process, very active geomorphically, emerged when flow concentrated in a single channel and met the fine subsurface layer, then rapidly and very efficiently exporting sediment downstream. Bedload transport intensity was the highest during this phase. Flows over the smooth subsurface tended to have higher Fr numbers than over paved multi-thread morphologies (compare Fig. 3e & f). Flows were thus generally supercritical during incision phases. Such single-channel morphologies were rare, occurring two or three times during each run, and never lasting more than a few minutes. During this phase, channels usually looked like plane bed configurations. Standing waves influenced by lateral shock waves were also the main flow hydraulics (Fig. 1a). Sediment was efficiently transported downstream of the former accumulation, building lobes further downstream or exporting sediment at the flume outlet (Fig. 3 and see video in supplementary material). Secondary flow paths formed on the sides of the main channels, usually with subcritical conditions due to their shallowness. These involved shallow depths and low velocities, and therefore smaller fluxes of water.

3.2 Froude number, slope and transport stage

Every point of the 61 flow reconstruction operations coming from 13 different runs was gathered in one data set with 1.7 million data points (Table 2). Each point is assumed to be representative of a 5-mm pixel in one of the 61 instantaneous pictures of the experiment. These data depict great variability in morphologies, slopes, grain sorting state, stage in the hydrograph, discharges and so on. The full data set is assumed to represent an integrated image of our analog model of debris flood deposition in unconfined reaches. Nonetheless, one must keep in mind that since every measurement is local, in a 2D depth-averaged sense, we expect that they locally capture high and low parameter values that would be averaged in a similar 1D, i.e., cross-sectional analysis. Parameter values are thus theoretically scattered over wider ranges than if the analysis had been performed in 1D. Comparing 1D and 2D estimates would be an interesting study that is beyond the scope of this paper: it would imply automatic detection of channels and bars, which is complicated in the experience of the authors.

Note that measurements taken using the two different sediment mixtures are pooled in the same data set because similar sorting and bedform patterns, as well as associated flow regimes and range of depths, were observed, although slightly steeper slopes were measured on the coarsest mixture (Piton 2016).

Froude numbers of the full data set are plotted against local slope extracted along the stream lines in Figure 4. Most data are within the range $0.02 < S < 0.2$. The Froude numbers increase as slope increases in channels with a slope milder than ≈ 0.1 . In contrast, a superior envelope, inversely correlated with the slope, appears for $S \gtrsim 0.1$. We expected that decreasing Froude numbers would occur with increasing slope as a direct consequence of increasing roughness, smaller and shallower channels, flow spreading and emergence of several associated energy dissipation processes such as hydraulic jumps, lateral shocks, breaking standing waves and so on. Both geomorphology and hydraulics are intrinsically coupled during this process.

To better highlight the coupled hydraulic and geomorphic processes, we filtered these overall results to focus on morphologically active channels where flows are competent and thus able to sculpt the channel's shape and structure, i.e., in active mobile bed channels. To assess the channel's capacity to adjust its morphology, the transport stage was computed, i.e., τ^*/τ_{cr}^* , with τ_{cr}^* the critical Shields parameter for incipient motion of sediment. Many values have been proposed for τ_{cr}^* : Shields 1936 proposed 0.06, while Meyer-Peter and Müller 1948 proposed 0.047. Recent research suggests that this parameter is slope-dependent (Mueller et al. 2005; Lamb et al. 2008; Recking 2009). Recking et al. (2008) proposed the following equation:

$$\tau_{cr}^* = 0.15 \times S^{0.275} \quad (5)$$

Equation (5) results for instance in $\tau_{cr}^* = 0.051$, 0.080 and 0.096 for slopes of 0.02, 0.1 and 0.2 (m/m), respectively.

sub-samples with $\tau^*/\tau_{cr}^* > 1$ were extracted from the full data set considering the τ_{cr}^* values of Shields 1936, Meyer-Peter and Müller 1948 and Recking et al. (2008) (Fig. 4c-e). The Froude numbers of each sub-sample are plotted as boxplots and distributions (Figure 5 and 6). We use different values of τ_{cr}^* in order to examine Froude number response irrespective of the specific equation employed. Some transport may occur in all channels approaching $\tau^*/\tau_{cr}^* \approx 1$ and that the higher the definition of τ_{cr}^* , the more likely the bedload transport is sufficient to rapidly adjust the channel forms. In addition, since the critical Shields parameter is computed here for D_{84} ,

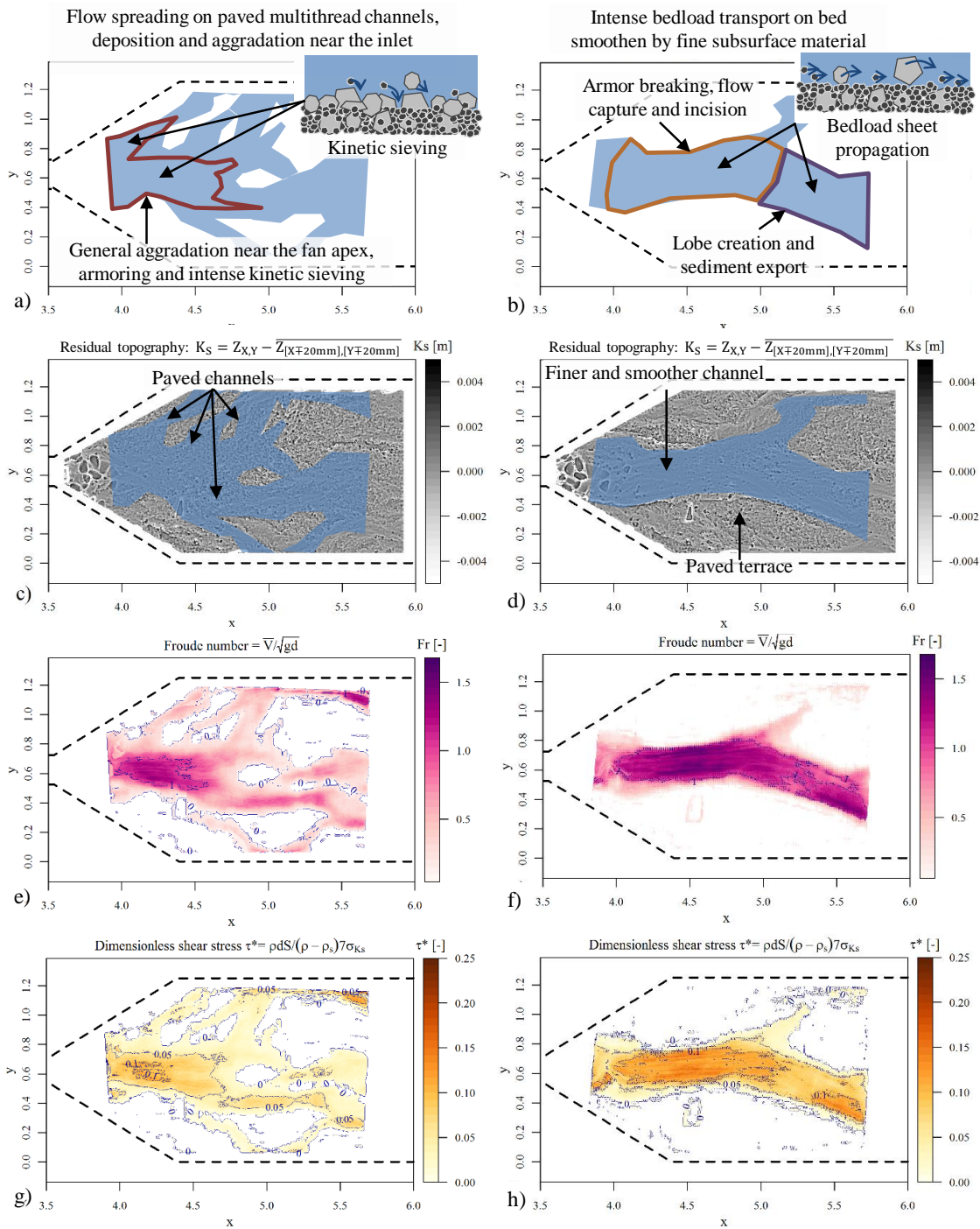


Figure 3: Conceptual top views of two geomorphic patterns: (a) a multi-thread channel experiencing aggradation and (b) an single-thread channel experiencing incision; residual topography measurement of both (c & d), Froude number spatial distribution of both (e & f) and Shields number spatial distribution of both (g & h). The single-thread channel indicates the flows shown in Figure 1

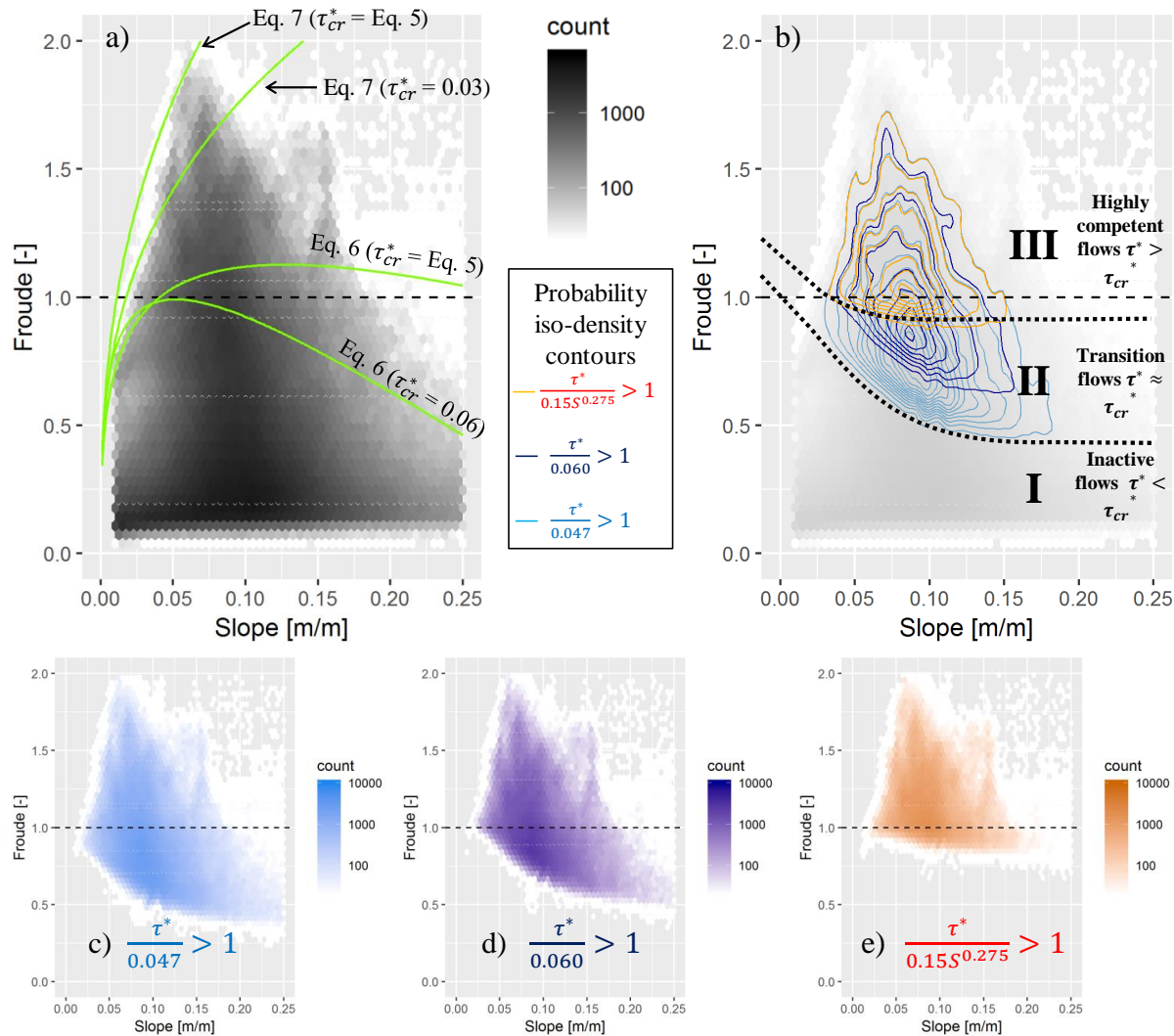


Figure 4: Froude number vs slope: a) full data set, b) conceptual view highlighting transport capacity domains based on transport stage (τ^*/τ_{cr}^*), full data set with colored probability density contours of sub-samples with transport stage higher than unity for various critical Shields values. Domains with τ^*/τ_{cr}^* lower than unity, close to unity and higher than unity are displayed with numbers "I", "II" and "III", respectively. Note that the sharp boundary represented by the dotted lines, eye-fitted, are not based on a clearly defined threshold and are actually progressive transitions; sub-samples selected with $\tau^*/\tau_{cr}^* > 1$ assuming c) $\tau_{cr}^* = 0.047$ (Meyer-Peter and Müller 1948) , d) $\tau_{cr}^* = 0.060$ (Shields 1936) and e) Eq. 5 (Recking et al. 2008). Most flows are subcritical, although the morphologically slightly active flows tend to have a near-critical Froude number and very active flow to obtain slightly supercritical flows. A superior envelope inversely correlated with slope appear: we assume that decreasing Froude numbers on increasing slopes are the print of increasing roughness and flow spreading with increasing slope, feedback from geomorphology on hydraulics

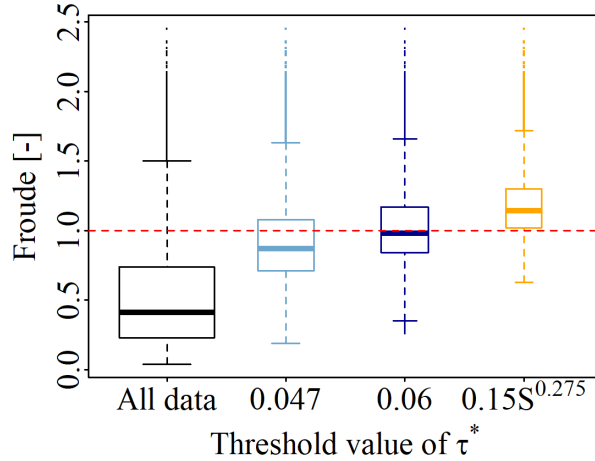


Figure 5: Synthetic Froude number statistics of the complete data set (1.7 million data points) and filtered with several Shields number threshold values, highlighting that morphologically active flows approach a critical Froude number. The boxplot to the right-hand side is filtered using the slope-dependent value of critical Shields number of Eq. (5)

Table 2: Froude number average and quantile values of sub-samples extracted with various threshold values of τ_{cr}^* and displayed in Figure 6

Shields threshold value	Froude average	Quantiles						Number of data $\times 10^6$
		5%	10%	50%	90%	95%	99%	
All data	0.52	0.14	0.16	0.41	1.04	1.22	1.51	1.7
>0.047	0.91	0.52	0.59	0.87	1.30	1.42	1.65	0.6
>0.060	1.01	0.63	0.71	0.97	1.36	1.47	1.69	0.43
>Eq. (5)	1.13	0.62	0.92	1.12	1.45	1.55	1.75	0.26

Shields stresses and thus transport stage are lower than they might be if using D_{50} , for instance. As a consequence, there is still sediment transport and possible morphological adjustments for $\tau^*/\tau_{cr}^* > 1$, although of lower intensity (MacKenzie et al. 2018). It has now been established that bedload transport of poorly sorted sediment does not show a sharp transition between static and mobile conditions, but rather a pseudo-cyclic and progressive shift toward partial and finally full mobility (Wilcock and McArdell 1997; Bacchi et al. 2014).

Most of our flow data correspond to relatively shallow flows with low τ^*/τ_{cr}^* values, which are subcritical despite the steepness of the channels (Fig. 5 - left box plot; Fig. 6 upper panel; Table 2). Sub-samples with higher threshold values τ_{cr}^* hold data coming from increasingly competent channels. Interestingly, higher threshold values τ_{cr}^* are correlated with higher Froude number ranges (Fig. 4c-e, 5 and 6). Thus, in the continuous transition between inactive to morphologically active flows, the Froude number increases with the transport stage. More interestingly, the highest Froude number values seldom exceed $\approx 1.5 - 2$ and ts with $\tau^*/\tau_{cr}^* > 1$ have near-critical Froude number values. High Froude numbers were not reached: the 95% and 99% quantiles of the full data set were 1.2 and 1.5, respectively (Table 2). Since the flow energy is minimum for critical flows (Grant 1997), it seems that the channel morphology approaches this optimum providing that the flows have a sufficient transport capacity to adjust the bed morphology, i.e., sufficiently high τ^*/τ_{cr}^* .

3.3 Comparison with theoretical equations

Using a near-threshold channel hypothesis, i.e., $\tau^* \approx \tau_{cr}^*$ and a Keulegan-type friction law, Grant 1997, proposed the following equation for Froude numbers at incipient motion:

$$Fr = 2.18 \left[\ln \left(\frac{1.65 \tau_{cr}^*}{S} \right) + 1.35 \right] S^{1/2} \quad (6)$$

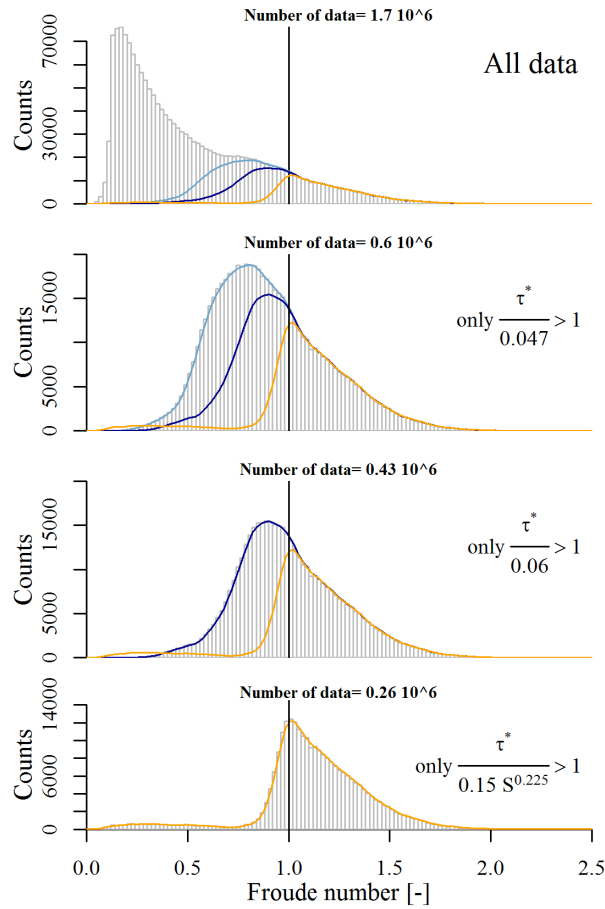


Figure 6: Froude number densities of the complete data set and sub-samples filtered with several critical Shields number threshold values. Each sub-sample is displayed with a different color to highlight how the different sub-samples relate to each other. The lower the threshold value, the more the sample includes subcritical Froude number values, although even in the sample filtered with Equation (5) (bottom panel), the most probable Froude number value is precisely critical

Conversely, using the hypothesis that $\tau^* \approx 1.4\tau_{cr}^*$ in gravel-bed channels and a Manning-Strickler type friction law resulted in the following equation:

$$Fr = 8.1 \left(\frac{1.4 (s - 1) \tau_{cr}^*}{\lambda} \right)^{1/6} S^{1/3} \quad (7)$$

with s the sediment density taken here as $2.65 \text{ (t/m}^3\text{)}$ and the λ coefficient to multiply by D_{50} to get the roughness height in the famous formulation $n \propto (d/\lambda D)^{-1/6}$ with the n Manning coefficient. In Grant (1997, Fig. 4), Eq. (6) gave a somewhat lower envelope of competent flows assuming $\tau_{cr}^* \approx 0.06$ while Eq. (7) gave a first approximation of the upper envelope assuming $\lambda = 6$ and $\tau_{cr}^* \approx 0.03$. Both equations are plotted in Fig. 4a along with updating using τ_{cr}^* values based on Eq. (5). Interestingly, while the Grant (1997, Fig. 4) covered roughly a slope range of 0–0.04, herein we push the slope range much further. Equation (6) remains near-critical for $S \approx 0.05 - 0.06$ and then correctly captures a decreasing trend with increasing slope. The argument that it is a reasonable border between domains "I" and "II", i.e., between inactive and near-critical flows, still holds. The updated version using slope-dependent τ_{cr}^* is higher but stays near-critical. Actually, the threshold for motion above a slope of 0.1–0.15, i.e., in debris flow reaches, becomes a complicated question involving both fluid mechanics and granular geomechanics; this theoretical development should be interpreted with caution.

In sum, within the range $S=0.02-0.1$, Eq. (6) seems a good first estimate of Fr for near-threshold channels, but one should still chose a definition for τ_{cr}^* . We recommend using the slope-dependent τ_{cr}^* of Eq. (5) which is based on more up-to-date results but is also representative of probably slightly more geomorphic activity according to our data. Equation (7) used with $\tau_{cr}^* \approx 0.03$ is consistent with Grant (1997) a first estimate of the upper envelope, though part of the percentile of data characterized by $Fr > 1.5$ is above it. Using slope-dependent τ_{cr}^* of Eq. (5) is a surprisingly accurate upper envelope. The hypothesis that gravel-bed channels remain in transport stages close to unity and rarely above ≈ 1.4 seems verified here here, assuming that the friction equation is correct. Note that the aforementioned decreasing trends for high slopes are not captured here. This is probably related to decreasing submergence at high slopes: Manning-Strickler formulations are not adapted for such low submergence (Ferguson 2007; Rickenmann and Recking 2011).

3.4 Correlation between Froude and Shields numbers

We find a clear positive correlation between Froude numbers and Shields numbers, as shown in Figure 7. The correlation coefficient between Fr and τ^* is 0.91 on the whole dataset. In essence and quite intuitively, since roughness is correlated with grain size (Eq. 1), the finer the bed, the smoother it is. The correspondence between high Fr (smooth bed) and high τ^* (fine bed) is the result. It is worth recalling (see previous section) that in our experiments high Fr numbers (high velocity, low depth) were always associated with armor breakup and very active transport above the subsurface finer material released by armor disruption. The underlying physical processes are discussed below. Supercritical flows occurring on the morphologically most active channels were transient in time because of fast geomorphic adjustments at these locations.

Most channel changes were progressive: flow generally shifted progressively from high to near threshold τ^* , i.e., from highly competent to transition flows. In other words, they shifted from Fig. 7b domain "III" to domain "I" via domain "II". The channel adjustments should therefore stop whenever flows achieved quasi-equilibrium between energy supply and dissipation as well as sediment supply and export. Assuming that quasi-equilibrium channels usually experience near threshold τ^* values (Grant 1997; Parker et al. 2007), according to Figure 7 these flows lie close below the critical Fr value (domain "II" in Fig. 7b). If the upstream sediment supply is significant enough to require a transport stage higher than 1, the flows may instead be near-critical (domain "I" in Fig. 7b). If deposition reaches a sufficiently high amount, the armor eventually breaks and flow passes through the fast phase of domain III, rapidly bringing the system back to domain II or I.

These results suggest that a self-stabilizing feedback loop emerges and limits the occurrence of high Fr values because the supercritical sample part is also the most morphologically active one: flows with high τ^* have a stronger capacity to rework their bed, adjusting it to increase friction, dissipate energy and approach the energetic optimum of critical flows.

4 Discussion

Grant (1997) speculated that supercritical flows should be rarely encountered in the field in mobile-bed river channels. During the reviewing process of the present paper and in light of more than 20 years of research, Gordon

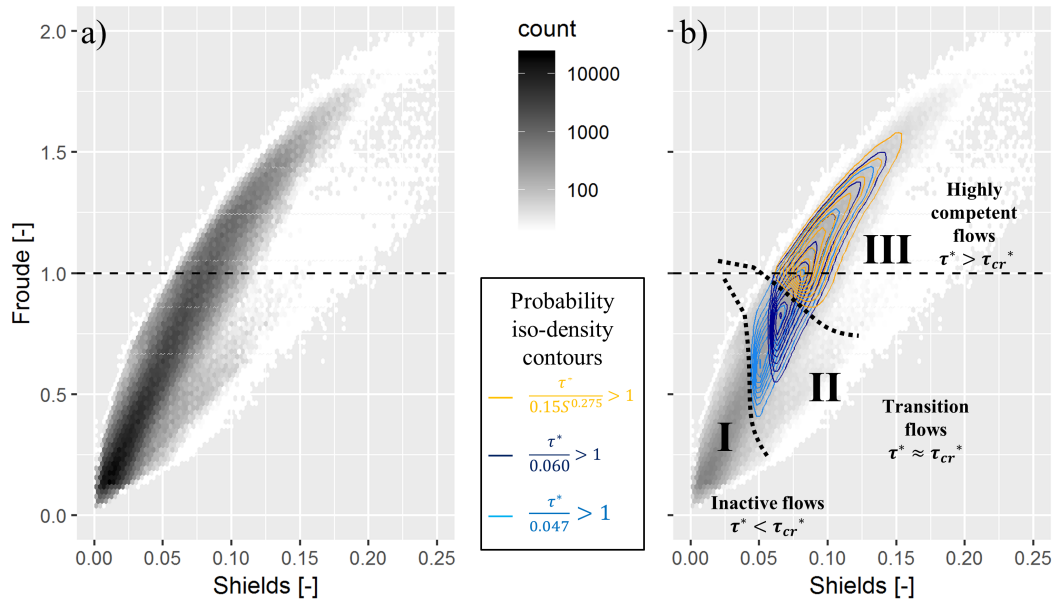


Figure 7: Froude number vs Shields number: a) Full data set ($r^2 = 0.91$) and b) main domains of transport stages with colored probability density contours of transport stage higher than unity for various critical Shields values: light blue $\tau_{cr}^* = 0.047$, dark blue $\tau_{cr}^* = 0.060$ and orange Eq. 5. Domains with transport stage lower than unity, close to unity and higher than unity are displayed with numbers "I", "II" and "III", respectively. Note that the sharp boundary represented by the dotted lines were simply eye-fitted and are actually progressive transitions. Transition flows are barely subcritical while competent flows are near critical to supercritical for high transport stages

Grant synthesized this, pointing out that "supercritical flows result in specific forms of energy dissipation (i.e., hydraulic jumps, standing waves) that extract energy from the flow and therefore reduce velocity back towards critical. In a sense, the flow is held in a tension between those forces that accelerate it towards (and locally above) critical and those forces that abstract energy, hence slow it down. Thus emerges the "strange attractor" at $Fr=1$. The ability of the flow to rework the bed is an important consideration in understanding how the channel adjusts over the long term to maintain near-critical flow conditions". This very clear description and the original paper adopt a rather hydraulically oriented perspective. Here, we broaden this argument based on experiment data to show that geomorphic adjustments, including adjustments of width, bed elevation, and armoring, are also mechanisms by which channels maintain near-critical flow conditions.

From a broader perspective, a number of regime theories or extremal equations have been proposed to define how alluvial channels adjust their slope and width to water and sediment supply. Huang et al. 2004 reviewed them in light of the "principle of minimum energy" and proposed ways to compute a theoretical optimal value for the width/depth ratio that would act as an attractor for a given discharge. They subsequently enlarged this approach, notably in Nanson and Huang 2008; Nanson and Huang 2016 with the "least action principle," attempting to propose a somewhat universal principle governing very long-term channel evolution based on a "mass-balance equilibrium". Although their working hypothesis was that the long-term form of a river channel mostly adjusts to convey the sediment load supplied to it, they agreed that flows having excessive energy, e.g., during a particularly high flood event, will adjust the channel geometry to dissipate it, usually by friction. Friction dissipation is driven by channel roughness and the width/depth ratio. Both can adjust at the time scale of a flood event, e.g., by bedform changes, armor breaking and bank erosion (Vaughn 1990; Righini et al. 2017; Scorpio et al. 2018). All rivers likely behave in this type of dynamic equilibrium, recovering from the last extreme flood event or shifting to a new state because of changes in boundary conditions (Rinaldi et al. 2011; Church and Ferguson 2015).

The assertion that a critical Froude number seems to be an attractor on a steep stream or upper bound at lower than formative flows has been consistently confirmed by hydraulics field measurements generally demonstrating subcritical or near-critical flow conditions in mountain streams (Tinkler 1997; Lenzi 2001; Zimmermann and Church 2001; Comiti et al. 2007; Comiti et al. 2009; Magirl et al. 2009; Nitsche et al. 2012; Recking et al. 2012; Schneider et al. 2015). Dramatic width adjustments in mountain rivers have regularly been reported in the literature after flood events (Rickenmann and Koschni 2010; Hauer and Habersack 2009; Ruiz-Villanueva et al. 2018). But still, Froude

numbers have seldom been reported to be highly supercritical. Amponsah et al. 2016, for instance, reported 35 measurements of peak discharges based on field measurements after a major flood that triggered major geomorphic adjustments in the Magra River system in Italy on 25th October 2011. Despite the high discharges ($10.6 \pm 7.8 \text{ m}^3 \cdot \text{s}^{-1} \cdot \text{km}^{-2}$, mean \pm standard deviation) and the relatively steep slopes (0.027 ± 0.021), all Froude numbers were estimated to be subcritical, although close to the critical value (0.75 ± 0.12).

In our experimental observations on very steep slopes, flows were consistently subcritical most of the time (Table 2). The morphologically active flows shift toward near-critical Froude numbers. This is consistent with a system adjusting its geometry and grain structure toward a minimum of energy. We conclude that Grant (1997)'s critical flow hypothesis seems to be correct as a first approximation when describing bedload-laden flows in alluvial channels that can self-adjust their channel structure and widths.

In very steep channels on mountain hill slopes, width is often constrained by large boulders or bedrock canyons (Church and Zimmermann 2007). Interestingly, even in these contexts the Froude number and slope do not systematically increase together. Conversely, a somewhat nonintuitive inverse correlation is experienced, as captured by Figure 4, where the Froude number decreases for slopes higher than 0.1. This correlation, still described in many papers notably in Grant (1997) or Schneider et al. (2015), but here accurately measured on a large data set, is the consequence of coupled hydraulic and geomorphic features of high gradient channels. Boulders and cobbles, supplied by colluvial processes and debris flows, greatly increase channel roughness (Piton and Recking 2017). Autogenic arrangements in cascade and step-pool morphologies increase energy dissipation even more since such bedforms are closely coupled and self-adjusted, with energy dissipating hydraulic processes such as hydraulic jumps and tumbling flows (Zimmermann et al. 2010). As pointed out by Grant 1997, such morphologies are often relics of formative discharges that, considering the bed material size and packing, rarely occur (Recking et al. 2012). Under inactive or weakly morphologically active flows, in a stream with a one-order-of-magnitude increase in slope, Schneider et al. (2015), for instance, measured Froude numbers lower in the $\approx 40\%$ -steep reach, compared to the milder, 3-4%-steep upstream reach. While the cascade bed in the steep reach generated huge friction and dissipation by hydraulic jumps, the milder plane bed was much smoother and allowed higher Fr to occur. Continuous field LSPIV measurement on a steep stream confirmed globally subcritical or near-critical flows (Ran et al. 2016). These observations demonstrate that in laterally confined channels, flow types and channel bed roughness can adjust quite effectively to limit supercritical flow occurrence. Bed widening is an additional degree of freedom of systems that are laterally unconfined, as in our experiments.

It is worth emphasizing however, that supercritical flows do exist in the field but are most often encountered in quite specific configurations:

- In laterally-constrained channels, e.g., bedrock channels (Vaughn 1990) or on alluvial fans where channels are artificially trained and width adjustment cannot occur. Le Boursicaud et al. 2016, for instance, measured a Froude number of approximately 2.6 (uncertainty range 2.0-3.8) in a 5-m-wide, 6.3%-steep cut stone-protected channel during pulsating bedload-laden flows (discharge: $22 \text{ m}^3/\text{s}$, uncertainty range 11-33 m^3/s). Asano and Uchida 2016 also observed supercritical flow in a laterally confined channel with a natural boulder and cobble-cover bed, 0.061-steep on average. A typhoon triggered a flood lasting several days where the Froude number reached 1.7 and 1.4 in the two sections, 5 and 8 m wide, respectively. The coarser bed likely reduced the Froude number compared to the cut-stone paved channel case reported in Le Boursicaud et al. 2016.
- At local flow constrictions, either natural or artificial, such as bridges. Using 1D and 2D modeling, Hauer and Habersack 2009 studied 17 reaches that experienced the 1000-year flood of the Kamp River (Austria) in 2002, which triggered major geomorphic changes in this 0.002- to 0.003-steep, gravel bed lowland river. Flows were indeed mostly subcritical but experienced supercritical transition at flow constriction sites.
- Over smooth beds loaded with fine sediment as observed by Montgomery et al. 1999 in 0.015- to 0.023-steep channels experiencing Froude numbers of 1.0-1.7 for flow depths of 0.03-0.05 m. These channels were particularly loaded with post-eruptive fine sediments (2-8 mm) from Mount Pinatubo (Philippines). It should be emphasized that Grant (1997) reported complementary measurements on one of these channels (Pasig-Potrero) at higher flow depths (0.16-0.22 m), which nonetheless flowed under channel average Froude numbers of about 1.1. Note that cobbles and coarser material are mentioned in the latter case: the fine material observed by Montgomery et al. 1999 could be considered a transient input, flushed relatively rapidly by the system.

This list is likely not exhaustive but points out typical configurations where supercritical flow can be expected. The clearest, most widely known examples of sustained supercritical flow are very steep smooth channels such as steep concrete-lined channels or dam spillways, i.e., particular configurations far from alluvial channels (Vaughn 1990; Boes and Hager 2003).

As pointed out by Gordon Grant during his review of the present paper, in essence, "the critical flow hypothesis does not require that flows are never supercritical, just that supercritical flow is likely to be a localized phenomenon and channels will - if given the chance - adjust towards critical". The "critical flow hypothesis" could have instead been called the "near-critical flow hypothesis" since flows are not strictly critical, as also discussed by Chanson 1998 and Tinkler 1999, but near critical since they are locally or transiently at most slightly supercritical or near-critical. Critical flows act as an attractor in sufficiently steep channels because it is energetically favorable and the physical processes coupling hydraulics and geomorphology naturally curtail situations much above $Fr = 1$ in mobile bed channels.

Reanalysis of past events for discharge estimations is a key application of this result. It can for instance refine the criterion related to Froude number used in the procedure of Lumbroso and Gaume (2012) to reconstruct flash-flood peak discharges in un-gauged basins. Other related applications in steep-slope streams during high flows include rapid estimation of discharge in ungauged basins, coarse measurement of discharge from remote sensing using width and surface velocity measurements. Another possible use of this result lies in channel assessment, for instance aiming at predicting whether or not bank erosion and width adjustments are likely. In cases where fixed-bed numerical models compute alluvial, laterally unconstrained reaches with very supercritical flows, i.e., $Fr > 1.3 - 1.5$, for a given discharge, the likelihood of bank erosion and width adjustments should, in our opinion, be considered high. Obviously, the higher the Fr , the higher the likelihood of adjustment. This hypothesis should be tested on field cases where grain size, width, discharge and depth data are available. This criterion could be useful, for instance, in studies trying to predict bed widening and extreme bedload-laden flood hazards as well as large wood recruitment by alluvial terrace erosion (Mazzorana et al. 2009; Comiti et al. 2016; Ruiz-Villanueva et al. 2016). In these studies, Froude number is a complementary parameter to the unit discharges and stream power still in use (Arnaud-Fassetta et al. 2005; Wohl and Jaeger 2009; Righini et al. 2017; Scorpio et al. 2018).

5 Conclusions

This paper explores a new data set of measurements taken on very steep flows, laden with bedload and laterally unconfined, at an unprecedented level of accuracy. In such contexts, flows can fully rework channels, easily adjusting width, depth and bed structure. A flow reconstruction procedure was used to compute depth as well as the Froude and Shields numbers on millions of pixels based on velocity, slope and roughness measurements. Despite steep slopes, mostly within the 0.02–0.2 range, surprisingly the Froude numbers were mostly subcritical. Subcritical Froude numbers were a consequence of naturally emerging standing waves and other energy dissipating features coupled with roughness adjustments: most channels were paved and/or their width increased triggering flow spreading on thinner, shallower layers. Competent flows, identified by the transport stage being higher than unity ($\tau^*/\tau_{cr}^* > 1$), were highlighted as near critical and seldom with $Fr > 1.3 - 1.5$. This demonstrates that, providing that bed structure and width can adjust, competent flows tend to rework channels and develop a flow pattern to approach the energy minimum of near-critical flows. This hypothesis was proposed by Grant 1997, has been confirmed by post-disaster flow computations on a few sections, but, to the best of our knowledge, until this study had not been demonstrated on such a large experimental sample. Considering near-critical flows during discharges high enough to be clearly competent in laterally unconfined beds therefore seems reasonable as a first approximation in steep gravel-bed channels.

Acknowledgments The data set is provided as supplemental data. The work of G.P. on this paper was funded by the H2020 project NAIAD [grant no. 730497] from the European Union's Horizon 2020 research and innovation program. The reviews of Chris S. Magirl, Francesco Comiti and Gordon Grant helped to significantly improve this paper. We are indebted to Gordon Grant for providing a number of tough but fair, acute and extremely complete critical remarks on several previous versions of this paper. A few of them were directly quoted in the paper to give credit where credit is due. We would like to thank also the editor-in-chief Amy East for her fast and excellent editorial work.

References

- Amponsah, W., Marchi, L., Zocatelli, D., Boni, G., Cavalli, M., Comiti, F., Crema, S., Lucía, A., Marra, F., and Borga, M. (2016). "Hydrometeorological Characterization of a Flash Flood Associated with Major Geomorphic Effects: Assessment of Peak Discharge Uncertainties and Analysis of the Runoff Response". *Journal of Hydrometeorology* 17.12, pp. 3063–3077. DOI: 10.1175/JHM-D-16-0081.1.

- Armanini, A. and Larcher, M. (2001). “Rational criterion for designing opening of slit-check dam”. *Journal of Hydraulic Engineering* 127.2, pp. 94–104. ISSN: 0733-9429. DOI: 10.1061/(ASCE)0733-9429(2001)127:2(94).
- Arnaud-Fassetta, G., Cossart, E., and Fort, M. (2005). “Hydro-geomorphic hazards and impact of man-made structures during the catastrophic flood of June 2000 in the Upper Guil catchment (Queyras, Southern French Alps)”. *Geomorphology* 66.1-4, pp. 41–67. DOI: 10.1016/j.geomorph.2004.03.014.
- Asano, Y. and Uchida, T. (2016). “Detailed documentation of dynamic changes in flow depth and surface velocity during a large flood in a steep mountain stream”. *Journal of Hydrology* 541, pp. 127–135. DOI: 10.1016/j.jhydro1.2016.04.033.
- Bacchi, V., Recking, A., Eckert, N., Frey, P., Piton, G., and Naaim, M. (2014). “The effects of kinetic sorting on sediment mobility on steep slopes”. *Earth Surface Processes and Landforms* 39.8, pp. 1075–1086. DOI: 10.1002/esp.3564.
- Boes, R. M. and Hager, W. H. (2003). “Hydraulic Design of Stepped Spillways”. *Journal of Hydraulic Engineering* 129.9, pp. 671–679. DOI: 10.1061/(asce)0733-9429(2003)129:9(671).
- Brasington, J., Vericat, D., and Rychkov, I. (2012). “Modeling river bed morphology, roughness, and surface sedimentology using high resolution terrestrial laser scanning”. *Water Resources Research* 48.11. DOI: 10.1029/2012wr012223.
- Cavalli, M., Tarolli, P., Marchi, L., and Fontana, G. D. (2008). “The effectiveness of airborne LiDAR data in the recognition of channel-bed morphology”. *CATENA* 73.3, pp. 249–260. DOI: 10.1016/j.catena.2007.11.001.
- Chanson, H. (1998). “Critical Flow in Rockbed Streams with Estimated Values for Manning’s n - Comment”. *Geomorphology* 25.3-4, pp. 279–282.
- Church, M and Ferguson, R. (2015). “Morphodynamics: Rivers beyond steady state”. *Water Resources Research* 51.4, pp. 1883–1897. DOI: 10.1002/2014WR016862.
- Church, M. and Zimmermann, A. (2007). “Form and stability of step-pool channels: Research progress”. *Water Resources Research* 43.3, p. 21. ISSN: 0043-1397. DOI: 10.1029/2006WR005037.
- Church, M. (2006). “Bed Material Transport and the Morphology of Alluvial River Channels”. *Annual Review of Earth and Planetary Sciences* 34.1, pp. 325–354. DOI: 10.1146/annurev.earth.33.092203.122721.
- Comiti, F., Mao, L., Wilcox, A., Wohl, E., and Lenzi, M. (2007). “Field-derived relationships for flow velocity and resistance in high-gradient streams”. *Journal of Hydrology* 340.1-2, pp. 48–62. ISSN: 0022-1694. DOI: 10.1016/j.jhydro1.2007.03.021.
- Comiti, F., Cadol, D., and Wohl, E (2009). “Flow regimes, bed morphology, and flow resistance in self-formed step-pool channels”. *Water Resources Research* 45.4. DOI: 10.1029/2008WR007259.
- Comiti, F., Lucía, A., and Rickenmann, D. (2016). “Large wood recruitment and transport during large floods: A review”. *Geomorphology* 269, pp. 23–39. DOI: 10.1016/j.geomorph.2016.06.016.
- Ferguson, R. (2007). “Flow resistance equations for gravel-and boulder-bed streams”. *Water Resources Research* 43.5, pp. 1–12. DOI: 10.1029/2006WR005422.
- Frey, P. and Church, M. (2009). “How river beds move”. *Science* 325.5947, pp. 1509–1510. ISSN: 00368075. DOI: 10.1126/science.1178516.
- Fujita, I., Muste, M., and Kruger, A. (1998). “Large-scale particle image velocimetry for flow analysis in hydraulic engineering applications.” *Journal of Hydraulic Research* 36(3), pp. 397–414. DOI: 10.1080/00221689809498626.
- Grant, G. (1997). “Critical flow constrains flow hydraulics in mobile-bed streams: A new hypothesis”. *Water Resources Research* 33.2, pp. 349–358. ISSN: 0043-1397. DOI: 10.1029/96WR03134.
- Hauer, C. and Habersack, H. (2009). “Morphodynamics of a 1000-year flood in the Kamp River, Austria, and impacts on floodplain morphology”. *Earth Surface Processes and Landforms* 34.5, pp. 654–682. DOI: 10.1002/esp.1763.
- Huang, H. Q., Chang, H. H., and Nanson, G. C. (2004). “Minimum energy as the general form of critical flow and maximum flow efficiency and for explaining variations in river channel pattern”. *Water Resources Research* 40.4. DOI: 10.1029/2003wr002539.
- Kuhnle, R. A. and Southard, J. B. (1988). “Bed load transport fluctuations in a gravel bed laboratory channel”. *Water Resources Research* 24.2, pp. 247–260. DOI: 10.1029/WR024i002p00247.
- Lamb, M. P., Dietrich, W. E., and Venditti, J. G. (2008). “Is the critical Shields stress for incipient sediment motion dependent on channel-bed slope?” *Journal of Geophysical Research: Earth Surface* 113.F2. DOI: 10.1029/2007JF000831.
- Le Boursicaud, R., Pénard, L., Hauet, A., Thollet, F., and Le Coz, J. (2016). “Gauging extreme floods on YouTube: Application of LSPIV to home movies for the post-event determination of stream discharges”. *Hydrological Processes* 30.1, pp. 90–105. DOI: 10.1002/hyp.10532.
- Lenzi, M. (2001). “Step-pool evolution in the Rio Cordon, Northeastern Italy”. *Earth Surface Processes and Landforms* 26.9, pp. 991–1008. ISSN: 0197-9337. DOI: 10.1002/esp.239.

- Liggett, J. A. (1993). “Critical Depth, Velocity Profiles, and Averaging”. *Journal of Irrigation and Drainage Engineering* 119.2, pp. 416–422. DOI: 10.1061/(asce)0733-9437(1993)119:2(416).
- Lumbroso, D. and Gaume, E. (2012). “Reducing the uncertainty in indirect estimates of extreme flash flood discharges”. *Journal of Hydrology* 414-415, pp. 16–30. DOI: 10.1016/j.jhydro.2011.08.048.
- MacKenzie, L. G., Eaton, B. C., and Church, M. (2018). “Breaking from the average: Why large grains matter in gravel-bed streams”. *Earth Surface Processes and Landforms*. DOI: 10.1002/esp.4465.
- Magirl, C. S., Gartner, J. W., Smart, G. M., and Webb, R. H. (2009). “Water velocity and the nature of critical flow in large rapids on the Colorado River, Utah”. *Water Resources Research* 45.5. DOI: 10.1029/2009wr007731.
- Mazzorana, B., Zischg, A., Largiader, A., and Hübl, J. (2009). “Hazard index maps for woody material recruitment and transport in alpine catchments”. *Natural Hazards and Earth System Science* 9.1, pp. 197–209. ISSN: 1561-8633. DOI: 10.5194/nhess-9-197-2009.
- Meyer-Peter, E. and Müller, R. (1948). “Formulas for bed-load transport”. *Proceedings of the 2nd Meeting of the International Association for Hydraulic Structures Research*. Delft: IAHR, pp. 39–64.
- Montgomery, D. R., Panfil, M. S., and Hayes, S. K. (1999). “Channel-bed mobility response to extreme sediment loading at Mount Pinatubo”. *Geology* 27.3, p. 271. DOI: 10.1130/0091-7613(1999)027<0271:cbmrte>2.3.co;2.
- Montgomery, D. and Buffington, J. (1997). “Channel-reach morphology in mountain drainage basins”. *Geological Society of America Bulletin* 109.5, pp. 596–611. ISSN: 00167802. DOI: 10.1130/0016-7606(1997)109<0596:CRMIMD>2.3.CO;2.
- Mueller, E. R., Pitlick, J., and Nelson, J. M. (2005). “Variation in the reference Shields stress for bed load transport in gravel-bed streams and rivers”. *Water Resources Research* 41.4. DOI: 10.1029/2004WR003692.
- Muste, M., Fujita, I., and Hauet, A. (2008). “Large-scale particle image velocimetry for measurements in riverine environments”. *Water Resources Research* 44.4, pp. 1–14. ISSN: 0043-1397. DOI: 10.1029/2008WR006950.
- Nanson, G. C. and Huang, H. Q. (2008). “Least action principle, equilibrium states, iterative adjustment and the stability of alluvial channels”. *Earth Surface Processes and Landforms* 33.6, pp. 923–942. DOI: 10.1002/esp.1584.
- Nanson, G. C. and Huang, H. Q. (2016). “Self-adjustment in rivers: Evidence for least action as the primary control of alluvial-channel form and process”. *Earth Surface Processes and Landforms* 42.4, pp. 575–594. DOI: 10.1002/esp.3999.
- Nitsche, M., Rickenmann, D., Kirchner, J., Turowski, J., and Badoux, A. (2012). “Macroroughness and variations in reach-averaged flow resistance in steep mountain streams”. *Water Resources Research* 48.12, pp. 1–16. ISSN: 0043-1397. DOI: 10.1029/2012WR012091.
- Parker, G., Wilcock, P., Paola, C., Dietrich, W., and Pitlick, J. (2007). “Physical basis for quasi-universal relations describing bankfull hydraulic geometry of single-thread gravel bed rivers”. *Journal of Geophysical Research: Earth Surface* 112.4, pp. 1–21. DOI: 10.1029/2006JF000549.
- Peakall, J., Ashworth, P., and Best, J. (1996). “Physical Modelling in Fluvial Geomorphology: Principles, Applications and Unresolved Issues”. *The Scientific Nature of Geomorphology: Proceedings of the 27th Binghamton Symposium in Geomorphology*. Ed. by B. L. Rhoads and C. E. Thorn. John Wiley Sons Ltd. URL: <http://books.google.fr/books?id=WtRNQUI9aS8C>.
- Piton, G. (2016). “Sediment transport control by check dams and open check dams in Alpine torrents”. PhD thesis. IRSTEA - Centre de Grenoble: Univ. Grenoble Alpes, p. 222. URL: <https://tel.archives-ouvertes.fr/tel-01420209>.
- Piton, G. and Recking, A. (2016). “Design of sediment traps with open check dams. I: hydraulic and deposition processes”. *Journal of Hydraulic Engineering* 142.2, pp. 1–23. DOI: 10.1061/(ASCE)HY.1943-7900.0001048.
- Piton, G. and Recking, A. (2017). “The concept of travelling bedload and its consequences for bedload computation of mountain streams”. *Earth Surface Processes and Landforms* 42.10, pp. 1505–1519. DOI: 10.1002/esp.4105.
- Piton, G., Mejean, S., Bellot, H., Le Guern, J., Carbonari, C., and Recking, A. (2016). “Bed-load trapping in open check dam basins measurements of flow velocities and depositions patterns”. *INTERPRAEVENT Conference proceedings*. Ed. by G. Koboltschnig, pp. 808–817.
- Piton, G., Fontaine, F., Bellot, H., Liébault, F., Bel, C., Recking, A., and Hugerot, T. (2018a). “Direct field observations of massive bedload and debris flow depositions in open check dams”. *E3S Web of Conferences*. Ed. by A. Paquier and N. Rivière. Vol. 40. EDP Sciences. Chap. 03003, pp. 1–8. DOI: 10.1051/e3sconf/20184003003.
- Piton, G., Recking, A., Le Coz, J., Bellot, H., Hauet, A., and Jodeau, M. (2018b). “Reconstructing Depth-Averaged Open-Channel Flows Using Image Velocimetry and Photogrammetry”. *Water Resources Research* 54 (6), pp. 4164–4179. DOI: 10.1029/2017WR021314.

- Polatel, C. (2006). “Large-Scale Roughness Effect On Free-Surface And Bulk Flow Characteristics In Open-channel Flows”. PhD thesis. University of Iowa.
- Rainato, R., Mao, L., García-Rama, A., Picco, L., Cesca, M., Vianello, A., Preciso, E., Scussel, G., and Lenzi, M. (2016). “Three decades of monitoring in the Rio Cordon instrumented basin: Sediment budget and temporal trend of sediment yield”. *Geomorphology* 291, pp. 45–56. ISSN: 0169-555X. DOI: 10.1016/j.geomorph.2016.03.012.
- Ran, Q.-h., Li, W., Liao, Q., Tang, H.-l., and Wang, M.-y. (2016). “Application of an automated LSPIV system in a mountainous stream for continuous flood flow measurements”. *Hydrological Processes* 30.17, pp. 3014–3029. DOI: 10.1002/hyp.10836.
- Recking, A. (2009). “Theoretical development on the effects of changing flow hydraulics on incipient bed load motion”. *Water Resources Research* 45.4, pp. 1–16. ISSN: 0043-1397. DOI: 10.1029/2008WR006826.
- Recking, A., Frey, P., Paquier, A., Belleudy, P., and Champagne, J. (2008). “Feedback between bed load and flow resistance in gravel and cobble bed rivers”. *Water Resources Research* 44.8, pp. 1–21. ISSN: 0043-1397. DOI: 10.1029/2008WR007272.
- Recking, A., Frey, P., Paquier, A., and Belleudy, P. (2009). “An experimental investigation of mechanisms involved in bed load sheet production and migration”. *Journal of Geophysical Research B: Solid Earth* 114.3, pp. 1–13. ISSN: 01480227. DOI: 10.1029/2008JF000990.
- Recking, A., Leduc, P., Liébault, F., and Church, M. (2012). “A field investigation of the influence of sediment supply on step-pool morphology and stability”. *Geomorphology* 139-140, pp. 53–66. ISSN: 0169-555X. DOI: 10.1016/j.geomorph.2011.09.024.
- Reitz, M. and Jerolmack, D. (2012). “Experimental alluvial fan evolution: Channel dynamics, slope controls, and shoreline growth”. *Journal of Geophysical Research F: Earth Surface* 117.2, pp. 1–19. ISSN: 01480227. DOI: 10.1029/2011JF002261.
- Rickenmann, D. and Koschni, A. (2010). “Sediment loads due to fluvial transport and debris flows during the 2005 flood events in Switzerland”. *Hydrological Processes* 24.8, pp. 993–1007. DOI: 10.1002/hyp.7536.
- Rickenmann, D. and Recking, A. (2011). “Evaluation of flow resistance in gravel-bed rivers through a large field data set”. *Water Resources Research* 47.7, pp. 1–22. ISSN: 0043-1397. DOI: 10.1029/2010WR009793.
- Rickenmann, D., Badoux, A., and Hunzinger, L. (2015). “Significance of sediment transport processes during piedmont floods: The 2005 flood events in Switzerland”. *Earth Surface Processes and Landforms* 41.2, pp. 224–230. DOI: 10.1002/esp.3835.
- Rickenmann, D., Turowski, J. M., Fritschi, B., Wyss, C., Laronne, J., Barzilai, R., Reid, I., Kreisler, A., Aigner, J., Seitz, H., and Habersack, H. (2013). “Bedload transport measurements with impact plate geophones: comparison of sensor calibration in different gravel-bed streams”. *Earth Surface Processes and Landforms* 39.7, pp. 928–942. DOI: 10.1002/esp.3499.
- Righini, M., Surian, N., Wohl, E., Marchi, L., Comiti, F., Amponsah, W., and Borga, M. (2017). “Geomorphic response to an extreme flood in two Mediterranean rivers (northeastern Sardinia, Italy): Analysis of controlling factors”. *Geomorphology* 290, pp. 184–199. DOI: 10.1016/j.geomorph.2017.04.014.
- Rinaldi, M., Piégay, H., and Surian, N. (2011). “Geomorphological approaches for river management and restoration in Italian and French Rivers”. *Geophysical Monograph Series* 194, pp. 95–113. DOI: 10.1029/2010GM000984.
- Ruiz-Villanueva, V., Piégay, H., Gurnell, A. M., Marston, R. A., and Stoffel, M. (2016). “Recent advances quantifying the large wood dynamics in river basins: New methods and remaining challenges”. *Reviews of Geophysics* 54.3, pp. 611–652. DOI: 10.1002/2015rg000514.
- Ruiz-Villanueva, V., Badoux, A., Rickenmann, D., Böckli, M., Schläfli, S., Steeb, N., Stoffel, M., and Rickli, C. (2018). “Impacts of a large flood along a mountain river basin: the importance of channel widening and estimating the large wood budget in the upper Emme River (Switzerland)”. *Earth Surface Dynamics* 6.4, pp. 1115–1137. DOI: 10.5194/esurf-6-1115-2018.
- Schneider, J., Rickenmann, D., Turowski, J., and Kirchner, J. (2015). “Self-adjustment of stream bed roughness and flow velocity in a steep mountain channel”. *Water Resources Research* 51.10, pp. 7838–7859. DOI: 10.1002/2015WR016934.
- Scorpio, V., Crema, S., Marra, F., Righini, M., Ciccacese, G., Borga, M., Cavalli, M., Corsini, A., Marchi, L., Surian, N., and Comiti, F. (2018). “Basin-scale analysis of the geomorphic effectiveness of flash floods: A study in the northern Apennines (Italy)”. *Science of The Total Environment* 640-641, pp. 337–351. DOI: 10.1016/j.scitotenv.2018.05.252.
- Shields, A. (1936). *Application of similarity principles and turbulence research to bed load movement*. Ed. by S. C.S. C. Laboratory. California Institute of Technology, Pasadena, CA.: U.S. Dept. of Agriculture. URL: <http://resolver.caltech.edu/CaltechKHR:HydroLabpub167>.

- Theule, J. I., Crema, S., Marchi, L., Cavalli, M., and Comiti, F. (2018). “Exploiting LSPIV to assess debris-flow velocities in the field”. *Natural Hazards and Earth System Sciences* 18.1, pp. 1–13. DOI: 10.5194/nhess-18-1-2018.
- Tinkler, K. J. (1999). “Critical flow in rockbed streams with estimated values for Manning’s n-Reply”. *Geomorphology* 25.3, p. 283.
- Tinkler, K. (1997). “Critical flow in rockbed streams with estimated values for Mannings n”. *Geomorphology* 20.1-2, pp. 147–164. DOI: 10.1016/S0169-555X(97)00011-1.
- Van Dijk, M., Kleinhans, M., Postma, G., and Kraal, E. (2012). “Contrasting morphodynamics in alluvial fans and fan deltas: Effect of the downstream boundary”. *Sedimentology* 59.7, pp. 2125–2145. ISSN: 00370746. DOI: 10.1111/j.1365-3091.2012.01337.x.
- Van Dijk, M., Postma, G., and Kleinhans, M. (2009). “Autocyclic behaviour of fan deltas: An analogue experimental study”. *Sedimentology* 56.5, pp. 1569–1589. ISSN: 00370746. DOI: 10.1111/j.1365-3091.2008.01047.x.
- Vaughn, D. M. (1990). “Flood dynamics of a concrete-lined, urban stream in Kansas City, Missouri”. *Earth Surface Processes and Landforms* 15.6, pp. 525–537. DOI: 10.1002/esp.3290150605.
- Vázquez-Tarrió, D., Borgniet, L., Liébault, F., and Recking, A. (2017). “Using UAS optical imagery and SfM photogrammetry to characterize the surface grain size of gravel bars in a braided river (Vénéon River, French Alps)”. *Geomorphology* 285, pp. 94–105. DOI: 10.1016/j.geomorph.2017.01.039.
- Venditti, J., Dietrich, W., Nelson, P., Wyzdga, M., Fadde, J., and Sklar, L. (2010). “Effect of sediment pulse grain size on sediment transport rates and bed mobility in gravel bed rivers”. *Journal of Geophysical Research F: Earth Surface* 115.3, pp. 1–19. DOI: 10.1029/2009JF001418.
- Westoby, M., Brasington, J., Glasser, N., Hambrey, M., and Reynolds, J. (2012). “Structure-from-Motion photogrammetry: A low-cost, effective tool for geoscience applications”. *Geomorphology* 179, pp. 300–314. DOI: 10.1016/j.geomorph.2012.08.021.
- Wilcock, P. and McArdell, B. (1997). “Partial transport of a sand/gravel sediment”. *Water Resources Research* 33.1, pp. 235–245. DOI: 10.1029/96WR02672.
- Wohl, E. and Jaeger, K. (2009). “A conceptual model for the longitudinal distribution of wood in mountain streams”. *Earth Surface Processes and Landforms* 34.3, pp. 329–344. ISSN: 0197-9337. DOI: 10.1002/esp.1722.
- Wolman, M. G. (1954). “A method of sampling coarse bed material”. *Transactions of American Geophysical Union* 35, pp. 951–956. DOI: 10.1029/TR035i006p00951.
- Zimmermann, A. and Church, M. (2001). “Channel morphology, gradient profiles and bed stresses during flood in a step-pool channel”. *Geomorphology* 40.3-4, pp. 311–327. ISSN: 0169-555X. DOI: 10.1016/S0169-555X(01)00057-5.
- Zimmermann, A., Church, M., and Hassan, M. A. (2010). “Step-pool stability: Testing the jammed state hypothesis”. *Journal of Geophysical Research: Earth Surface* 115.F2. DOI: 10.1029/2009jfe001365.